THE ASTROPHYSICAL JOURNAL, 567:532–543, 2002 March 1

THE NUCLEOSYNTHETIC SIGNATURE OF POPULATION III

A. HEGER AND S. E. WOOSLEY
Department of Astronomy and Astrophysics, University of California at Santa Cruz, 477 Clark Kerr Hall, Santa Cruz, CA 95064;
alex@ucolick.org, woosley@ucolick.org
Received 2001 July 2; accepted 2001 November 5

ABSTRACT

Growing evidence suggests that the first generation of stars may have been quite massive ($\sim$100–300 $M_\odot$). Could these stars have left a distinct nucleosynthetic signature? We explore the nucleosynthesis of helium cores in the mass range $M_{\rm He} = 64$–$133\ M_\odot$, corresponding to main-sequence star masses of approximately 140–260 $M_\odot$. Above $M_{\rm He} = 133\ M_\odot$, without rotation and using current reaction rates, a black hole is formed, and no nucleosynthesis is ejected. For lighter helium core masses, $\sim$40–63 $M_\odot$, violent pulsations occur, induced by the pair instability and accompanied by supernova-like mass ejection, but the star eventually produces a large iron core in hydrostatic equilibrium. It is likely that this core, too, collapses to a black hole, thus cleanly separating the heavy-element nucleosynthesis of pair instability supernovae from those of other masses, both above and below. Indeed, black hole formation is a likely outcome for all Population III stars with main-sequence masses between about 25 and 140 $M_\odot$ ($M_{\rm He} = 9$–$63\ M_\odot$) as well as those above 260 $M_\odot$. Nucleosynthesis in pair instability supernovae varies greatly with the mass of the helium core. This core determines the maximum temperature reached during the bounce. At the upper range of exploding core masses, a maximum of 57 $M_\odot$ of ^{56}Ni is produced, making these the most energetic and the brightest thermonuclear explosions in the universe. Integrating over a distribution of masses, we find that pair instability supernovae produce a roughly solar distribution of nuclei having even nuclear charge (Si, S, Ar, etc.) but are remarkably deficient in producing elements with odd nuclear charge—Na, Al, P, V, Mn, etc. This is because there is no stage of stable post–helium burning to set the neutron excess. Also, essentially no elements heavier than zinc are produced owing to a lack of *s*- and *r*-processes. The Fe/Si ratio is quite sensitive to whether the upper bound on the initial mass function is over 260 $M_\odot$ or somewhere between 140 and 260 $M_\odot$. When the yields of pair instability supernovae are combined with reasonable estimates of the nucleosynthesis of Population III stars from 12 to 40 $M_\odot$, this distinctive pattern of deficient production of odd-Z elements persists. Some possible strategies for testing our predictions are discussed.

Subject headings: nuclear reactions, nucleosynthesis, abundances — stars: early-type — supernovae: general
On-line material: machine-readable tables

1. INTRODUCTION

Simulations of the collapse of primordial molecular clouds suggest that the first generation of stars (Ostriker & Gnedin 1996) contained many massive members, from 100 up to 1000 $M_\odot$ (see, e.g., Larson 2000; Bromm, Coppi, & Larson 1999; Abel, Bryan, & Norman 2000). Calculations by Nakamura & Umemura (2001) suggest a bimodal initial mass function for Population III with peaks at $\sim$100 and 1–2 $M_\odot$. Considerable attention has been given recently to the nucleosynthesis of stars having main-sequence mass below 100 $M_\odot$ (Woosely & Weaver 1995; Thielemann, Nomoto, & Hashimoto 1996), but what is the nucleosynthetic signature of stars appreciably heavier?

For nonrotating stars over 260 $M_\odot$ on the main sequence, the answer is simple—zero (Fryer, Woosley, & Heger 2001). The nuclear energy released when the star collapses on the pair instability is not sufficient to reverse the implosion before the onset of the photodisintegration instability, and the star becomes a black hole (see also Rakavy, Shaviv, & Zinamon 1967; Bond, Arnett, & Carr 1984; Glatzel, Fricke, & El Eid 1985; Woosley 1986), sweeping all heavy-element production inside. Between approximately 140 and 260 $M_\odot$ lies the domain of pair instability supernovae. After central helium burning, stars have high enough central entropy that they enter a temperature and density regime in which electron/positron pairs are created in abundance, converting internal gas energy into rest mass of the pairs without contributing much to the pressure (Barkat, Rakavy, & Sack 1967; Bond, Arnett, & Carr 1984). When this instability is encountered, the star contracts rapidly until implosive oxygen and silicon burning, depending on the mass of the star, produce enough energy to revert the collapse. These objects are completely disrupted by nuclear-powered explosions. Unlike their lighter cousins, the explosion mechanism in pair instability supernovae is well understood, and there are no issues of "mass cut" or "fallback" to complicate the outcome. The stellar core implodes to a certain maximum temperature that depends on its mass, burns fuel explosively because of inertial overshoot, and then explodes. Provided that such stars existed and retained their high mass until death, the outcome (neglecting rotation) is uniquely calculable. It is thought that the precollapse winds and pulsations of such stars result in little mass loss (Kudritzki 2000; Baraffe, Heger, & Woosley 2001; Vink, de Koter, & Lamers 2001).

Nucleosynthesis in pair instability supernovae has been previously studied by Ober, El Eid, & Fricke (1983), Woolsey & Weaver (1982), and Woosley (1986), but those calculations examined a limited range of stellar masses and had very restricted nuclear reaction networks. In particular, the synthesis of rare elements with odd nuclear charge was not followed nor were species heavier than nickel.

Here we follow the evolution of 14 helium stars in the mass range 65–130 $M_\odot$ using a nuclear reaction networks of 304 (presupernova) and 477 (supernova) isotopes. The synthesis of isotopes at the boundaries of the networks is always sufficiently low to determine the yields of these objects completely. We also briefly describe the evolution of helium cores that are slightly larger (over 133.3 $M_\odot$) and slightly smaller (63 $M_\odot$) with the conclusion that black hole formation is likely in both cases. This allows one to separate cleanly the yields of pair instability supernovae from stars of slightly lower or higher mass. In the following sections we discuss our computational procedure and the nucleosynthetic results. In § 3.2 these results are integrated over an initial mass function (IMF) for comparison with observed abundances in very metal-deficient stars and clouds. The distinctive signature is a composition almost solar-like in the ratios among elements with even nuclear charge but lacking in elements with odd charge. We also discuss the possibility that the initial mass function is truncated somewhere short of $\sim 200\ M_\odot$, in which case the contribution to iron group nucleosynthesis from pair instability supernovae would be relatively small.

2. COMPUTATIONAL PROCEDURE AND ASSUMPTIONS

All calculations were carried out using the implicit hydrodynamics code KEPLER (Weaver, Zimmerman, & Woosley 1978; Heger, Langer, & Woosley 2000a). The equation of state allows for electrons and pairs of arbitrary degeneracy and relativity. The opacity was taken from Igelsias & Rogers (1996), and the principal nuclear reaction rates were as described by Rauscher et al. (2002). For the important $^{12}C(\alpha,\gamma)^{16}O$ reaction rate, we used Buchmann (1996) updated with Buchmann (2000, private communication; see also Caughlan & Fowler 1988; Kunz et al. 2001; Heger, Woosley, & Waters 2000b). Mass loss was not taken into account except what was driven by the pair instability pulsations studied here.

Nucleosynthesis was determined by "coprocessing" the stellar evolution model with a network of 304 isotopes prior to the explosion and 477 nuclei during in the explosion. The network contained all the necessary isotopes of elements from hydrogen to ruthenium. Trial calculations with a larger network showed that this network was adequate to correctly follow all species that accumulated to greater than 10^{-15} by mass fraction throughout the presupernova evolution and the explosion.

A series of helium core masses was then calculated, starting from the helium-burning main sequence and ending when either (1) an iron core formed in hydrostatic equilibrium and began to collapse on the photodisintegration instability, (2) a black hole was clearly about to form, or (3) the star was completely disrupted by an explosion. Our helium stars were presumed to consist initially of almost pure helium (Population III). A total of 25 helium cores were studied having masses 60, 63, 64, 65, 70, 75, 80, ..., 125, 130, 131, 132, 133, 133.3, 133.31, 134, 135, and 140 $M_\odot$. This spans the range of objects expected to become pair instability supernovae and explores the boundary of this range with good resolution. The initial composition (Table 1) used in all cases was that of a 200 $M_\odot$ Population III star (93 $M_\odot$ helium core) evolved from the hydrogen-burning main sequence to helium ignition. Some CNO isotopes formed as a consequence of 3α reactions on the main sequence (Ezer & Cameron 1971; Baraffe et al. 2001). The neutron excess of this starting composition, $\eta = \Sigma(N_i - Z_i)Y_i$, was 1.9×10^{-7}. A typical value of this parameter for solar metallicity stars at the onset of helium burning is 0.002. As we shall see, this change has dramatic consequences for the nucleosynthesis of odd-Z elements.

TABLE 1

INITIAL HELIUM CORE ABUNDANCES

Species	X	Species	X	Species	X
^{4}He	0.9998	^{12}C	2.0E−4	^{14}C	1.1E−7
^{14}N	2.0E−8	^{15}N	2.5E−9	^{16}O	3.1E−6
^{17}O	3.0E−8	^{18}O	1.0E−6	^{19}F	6.9E−9
^{20}Ne	4.2E−9	^{21}Ne	3.6E−10	^{22}Ne	6.7E−7
^{23}Na	4.1E−10	^{30}Si	1.3E−10	^{31}P	3.8E−10
^{32}S	1.2E−10	^{36}S	2.1E−10	^{38}Ar	1.1E−10

3. STELLAR MODELS AND YIELDS

Following helium burning, each stellar core consisted mostly of oxygen. For example, the mass fractions of ^{12}C and ^{16}O when the star reached a central temperature of 5×10^8 K were [0.10, 0.82], [0.089, 0.81], and [0.080, 0.80] for helium stars of 80, 100, and 120 $M_\odot$, respectively. The remainder was mostly ^{20}Ne and ^{24}Mg. The total oxygen masses in each of these three stars at this same point was 61.9, 77.0, and 91.6 $M_\odot$. The surface of each star remained nearly pure helium, but the helium mass fraction declined to 0.5 within 1.0 $M_\odot$ of the surface. Had mass loss been included, these would have become WC or WO stars.

Each star then proceeded to burn away its central carbon abundance—and then neon—radiatively. That is, no exoergic, convective core was formed. By the end of carbon burning the star had begun to encounter the pair instability, and by central neon depletion, typically at $(2.0–2.2) \times 10^9$ K, its carbon/oxygen core was collapsing at speeds in excess of 1000 km s^{-1}. Explosion followed, powered by explosive oxygen burning, and, for higher masses, additionally by explosive silicon burning. Bounce temperatures and densities for the 80, 100, and 120 $M_\odot$ models were 3.88, 4.53, and 5.39×10^9 K and 2.32, 3.20, and 5.42×10^6 g cm^{-3}, respectively. Table 2 gives the central temperature T_c density, ρ_c and the neutron, proton, and ^{4}He mass fractions at the time of highest central density. Figure 1 gives the explosion energy (kinetic energy at infinity) and bulk nucleosynthetic yields for all stars studied. Greater nucleosynthetic detail can be found in Table 3 and is discussed in § 3.2.

3.1. *Critical Masses: Stars at the Extreme*

Although the answer depends on the rate for $^{12}C(\alpha,\gamma)^{16}O$, the neglect of rotation, and possibly the convection model, we determined the range of helium core masses that become pair instability supernovae to be $\sim$64–133 $M_\odot$. This corresponds to main-sequence stars of approximately 140–260 $M_\odot$. An approximate empirical relation between the helium core mass and main-sequence mass in this mass range that we use here is

$$M_{\rm He} \approx \tfrac{13}{24}\,(M_{\rm ZAMS} - 20\ M_\odot)\,. \quad (1)$$

The 63 $M_\odot$ helium core had an interesting evolution that included three violent episodes of mass ejection spanning an interval of 5000 yr before finally settling down to burn silicon in hydrostatic equilibrium. The first collapse hap-

TABLE 2

CENTRAL PARAMETERS AT MAXIMUM DENSITY

Mass	T_c (K)	ρ_c (g cm^{-3})	$X(n)$	$X(p)$	$X(^4\mathrm{He})$	η_c
65	1.741×10^9	3.158×10^5	1.145×10^{-20}	9.808×10^{-17}	1.756×10^{-13}	2.905×10^{-4}
70	3.570×10^9	2.001×10^6	1.412×10^{-12}	2.356×10^{-4}	5.395×10^{-5}	2.812×10^{-4}
75	3.867×10^9	2.544×10^6	2.381×10^{-11}	9.438×10^{-4}	3.014×10^{-4}	2.892×10^{-4}
80	3.876×10^9	2.316×10^6	2.960×10^{-11}	1.040×10^{-3}	3.492×10^{-4}	2.583×10^{-4}
85	4.025×10^9	2.479×10^6	9.769×10^{-11}	2.370×10^{-3}	8.908×10^{-4}	2.400×10^{-4}
90	4.197×10^9	2.699×10^6	3.761×10^{-10}	5.328×10^{-3}	2.518×10^{-3}	2.636×10^{-4}
95	4.355×10^9	2.902×10^6	1.418×10^{-9}	8.919×10^{-3}	6.228×10^{-3}	2.959×10^{-4}
100.....	4.533×10^9	3.195×10^6	6.519×10^{-9}	1.325×10^{-2}	1.627×10^{-2}	3.746×10^{-4}
105.....	4.720×10^9	3.577×10^6	2.775×10^{-8}	1.743×10^{-2}	3.399×10^{-2}	4.705×10^{-4}
110.....	4.931×10^9	4.079×10^6	1.158×10^{-7}	2.144×10^{-2}	6.029×10^{-2}	5.643×10^{-4}
115.....	5.140×10^9	4.637×10^6	4.591×10^{-7}	2.460×10^{-2}	9.971×10^{-2}	7.311×10^{-4}
120.....	5.390×10^9	5.423×10^6	2.118×10^{-6}	2.688×10^{-2}	1.672×10^{-1}	9.632×10^{-4}
125.....	5.734×10^9	6.766×10^6	1.421×10^{-5}	2.757×10^{-2}	3.002×10^{-1}	1.317×10^{-3}
130.....	6.169×10^9	9.012×10^6	1.312×10^{-4}	2.356×10^{-2}	5.312×10^{-1}	1.867×10^{-3}

pened, as in other pair-unstable stars, just after helium burning. The center of the star reached a temperature of 3.2×10^9 K and density 1.5×10^6 g cm^{-3} before rebounding in an energetic explosion that released 6.5×10^{51} ergs from nuclear burning, principally explosive oxygen burning (4.5×10^{51} ergs was released above a central temperature of 3×10^9 K; 6.4×10^{51} ergs was released above 2×10^9 K; 6.5×10^{51} ergs is the net energy release after nuclear burning first exceeded neutrino losses in the star). The total binding of the star actually became briefly positive at this point (6.9×10^{50} ergs), but the outward motion was hydrodynamically concentrated into the outer layers with the result that only 12.8 $M_\odot$ was ejected with kinetic energy 1.2×10^{51} ergs, the equivalent of an ordinary Type II supernova. The remaining star then experienced an extended period of Kelvin-Helmholtz contraction during which no fuel was burned, but the central temperature and density gradually rose. This contraction phase after the first "pulse" was slow because temperature and density at the stellar center after expansion ($\rho = 25$ g cm^{-3}; $T = 7.3 \times 10^7$ K) were too low for neutrino emission. Thus, the star contracted on the Kelvin-Helmholtz timescale for photon emission from the surface and was unaffected by neutrino emission. During most of the next 4800 yr the star had a surface luminosity of (8–10) $\times 10^{39}$ ergs s^{-1}, and that luminosity governed the evolution until late times. However, the details of the re-expansion and, consequently, the timescale of the subsequent contraction phase may depend on the modeling of energy transport (convection/Rayleigh-Taylor instabilities) during the dynamic phases of the core. We assumed convection in subsonic regions.

A second collapse and explosion occurred 4800 yr after the first pulse, this time ejecting 2.7 $M_\odot$ with kinetic energy of only 1.3×10^{50} ergs. The star did not expand so much following this weak explosion, rebounding from a temperature of 3.68×10^9 K, $\rho = 1.0 \times 10^7$ g cm^{-3} to only 1.2×10^9 K and 4.9×10^5 g cm^{-3}. Neutrino losses rapidly robbed the core of energy so that the remaining star (now 47.5 $M_\odot$) evolved rapidly through a second Kelvin-Helmholtz phase. By this point the central 4 $M_\odot$ of the star

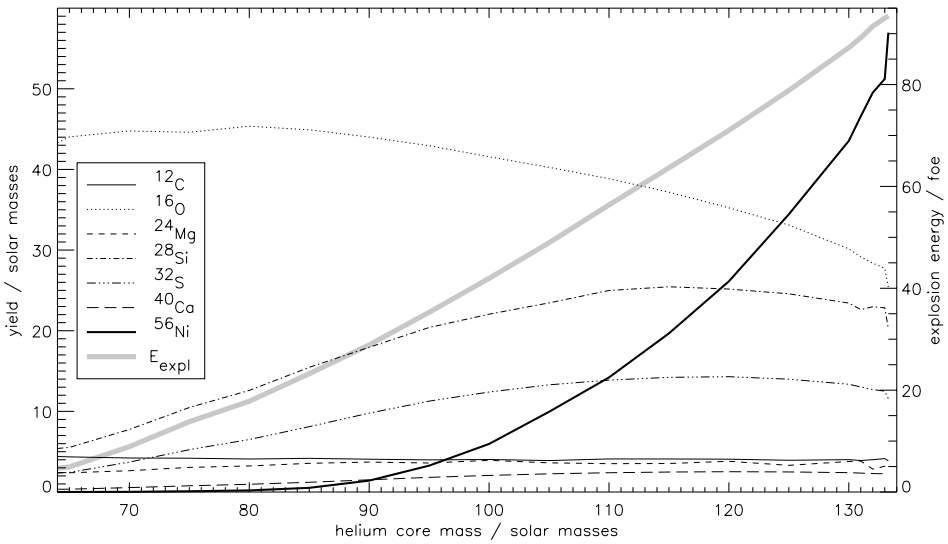

FIG. 1.—Yields of the dominant elements (*left-hand scale*) and explosion energies (*thick gray line*, *right-hand scale*; one "foe" is 10^{51} ergs, about the explosion energy of a typical modern supernova) as a function of helium core mass (see also Heger et al. 2001). The range shown corresponds to main-sequence masses of ~140–260 $M_\odot$. Helium cores of lower mass do not explode in a single pulse, and those of higher mass collapse into black holes (see Fig. 2).

TABLE 3

YIELDS (IN SOLAR MASSES)

Ion	65	70	75	80	85	90	95	100	105	110	115	120	125	130
^{4}He	1.96	1.55	1.44	1.46	1.44	1.41	1.42	1.47	1.53	1.66	1.77	2.00	2.38	2.82
^{12}C	6.89	4.54	4.32	4.33	4.28	4.21	4.13	4.01	3.85	3.74	3.73	3.71	3.61	3.49
^{13}C	2.33(− 7)	4.19(− 7)	7.44(− 7)	8.86(− 7)	8.48(− 7)	5.78(− 7)	3.59(− 7)	4.31(− 7)	2.30(− 7)	1.60(− 7)	1.64(− 7)	1.51(− 7)	1.38(− 7)	9.36(− 8)
^{14}N	7.84(− 5)	5.04(− 5)	4.31(− 5)	4.15(− 5)	3.78(− 5)	3.46(− 5)	3.23(− 5)	3.10(− 5)	2.92(− 5)	2.75(− 5)	2.42(− 5)	1.95(− 5)	1.41(− 5)	1.10(− 5)
^{15}N	7.27(− 7)	7.03(− 6)	6.69(− 6)	6.69(− 6)	6.57(− 6)	6.45(− 6)	6.41(− 6)	6.43(− 6)	6.51(− 6)	6.76(− 6)	6.99(− 6)	7.19(− 6)	7.03(− 6)	6.65(− 6)
^{16}O	4.92(1)	4.58(1)	4.44(1)	4.68(1)	4.66(1)	4.59(1)	4.52(1)	4.39(1)	4.27(1)	4.11(1)	3.98(1)	3.81(1)	3.59(1)	3.34(1)
^{17}O	4.27(− 6)	9.85(− 7)	7.76(− 7)	7.47(− 7)	6.60(− 7)	5.93(− 7)	5.38(− 7)	5.09(− 7)	4.73(− 7)	4.45(− 7)	4.13(− 7)	3.74(− 7)	3.26(− 7)	2.86(− 7)
^{18}O	2.81(− 6)	9.94(− 7)	8.50(− 7)	8.15(− 7)	7.94(− 7)	7.84(− 7)	7.63(− 7)	8.10(− 7)	7.99(− 7)	8.23(− 7)	8.35(− 7)	8.50(− 7)	8.89(− 7)	8.47(− 7)
^{19}F	1.63(− 8)	1.41(− 8)	1.28(− 8)	1.23(− 8)	1.23(− 8)	1.42(− 8)	1.61(− 8)	1.69(− 8)	1.93(− 8)	2.03(− 8)	2.40(− 8)	2.63(− 8)	2.76(− 8)	2.58(− 8)
^{20}Ne ...	4.99	4.04	3.89	4.22	4.20	4.10	3.98	4.06	3.86	3.90	3.84	3.88	3.92	3.73
^{21}Ne ...	5.04(− 4)	6.53(− 5)	2.10(− 4)	2.49(− 4)	2.99(− 4)	2.51(− 4)	1.82(− 4)	2.14(− 4)	1.42(− 4)	1.65(− 4)	1.45(− 4)	1.52(− 4)	1.68(− 4)	1.24(− 4)
^{22}Ne ...	1.86(− 4)	2.01(− 5)	1.85(− 5)	1.97(− 5)	2.19(− 5)	2.27(− 5)	2.26(− 5)	2.37(− 5)	2.28(− 5)	2.46(− 5)	2.39(− 5)	2.41(− 5)	2.32(− 5)	2.02(− 5)
^{23}Na ...	9.13(− 3)	3.14(− 3)	2.95(− 3)	3.02(− 3)	2.96(− 3)	2.88(− 3)	2.82(− 3)	2.76(− 3)	2.69(− 3)	2.66(− 3)	2.68(− 3)	2.74(− 3)	2.81(− 3)	2.78(− 3)
^{24}Mg ...	1.53	3.02	3.49	3.67	3.97	4.24	4.38	4.41	4.40	4.31	4.50	4.55	4.42	4.38
^{25}Mg ...	3.78(− 3)	1.08(− 3)	3.07(− 3)	2.23(− 3)	3.36(− 3)	4.15(− 3)	4.70(− 3)	4.27(− 3)	4.57(− 3)	4.55(− 3)	4.04(− 3)	3.76(− 3)	3.39(− 3)	3.56(− 3)
^{26}Mg ...	3.71(− 3)	1.74(− 3)	1.69(− 3)	1.73(− 3)	1.79(− 3)	1.92(− 3)	2.06(− 3)	1.92(− 3)	2.05(− 3)	1.91(− 3)	1.94(− 3)	1.86(− 3)	1.72(− 3)	1.73(− 3)
^{27}Al	3.37(− 2)	1.77(− 2)	1.66(− 2)	1.59(− 2)	1.67(− 2)	1.72(− 2)	1.77(− 2)	1.63(− 2)	1.66(− 2)	1.55(− 2)	1.50(− 2)	1.42(− 2)	1.29(− 2)	1.34(− 2)
^{28}Si	3.15(− 1)	7.97	1.22(1)	1.36(1)	1.65(1)	1.92(1)	2.14(1)	2.31(1)	2.45(1)	2.52(1)	2.57(1)	2.57(1)	2.51(1)	2.42(1)
^{29}Si	1.96(− 3)	2.32(− 2)	2.25(− 2)	2.22(− 2)	2.14(− 2)	2.07(− 2)	2.05(− 2)	1.94(− 2)	1.94(− 2)	1.81(− 2)	1.78(− 2)	1.68(− 2)	1.52(− 2)	1.49(− 2)
^{30}Si	6.52(− 3)	2.74(− 3)	1.47(− 3)	1.33(− 3)	1.23(− 3)	1.23(− 3)	1.36(− 3)	1.20(− 3)	1.45(− 3)	1.35(− 3)	1.43(− 3)	1.37(− 3)	1.17(− 3)	1.35(− 3)
^{31}P	2.71(− 3)	2.90(− 3)	2.16(− 3)	1.89(− 3)	1.64(− 3)	1.45(− 3)	1.36(− 3)	1.19(− 3)	1.23(− 3)	1.08(− 3)	1.17(− 3)	1.12(− 3)	9.53(− 4)	1.07(− 3)
^{32}S	9.50(− 4)	2.43	4.12	4.70	6.08	7.58	8.85	9.97	1.08(1)	1.14(1)	1.18(1)	1.20(1)	1.18(1)	1.14(1)
^{33}S	3.84(− 5)	3.07(− 3)	3.50(− 3)	3.64(− 3)	3.73(− 3)	3.75(− 3)	3.74(− 3)	3.68(− 3)	3.59(− 3)	3.47(− 3)	3.34(− 3)	3.18(− 3)	2.96(− 3)	2.71(− 3)
^{34}S	2.06(− 4)	6.36(− 3)	4.57(− 3)	2.94(− 3)	1.93(− 3)	1.22(− 3)	7.83(− 4)	4.98(− 4)	3.28(− 4)	2.12(− 4)	1.49(− 4)	1.08(− 4)	8.83(− 5)	9.78(− 5)
^{36}S	1.12(− 8)	1.12(− 8)	7.86(− 9)	6.60(− 9)	5.53(− 9)	4.55(− 9)	3.82(− 9)	3.24(− 9)	2.73(− 9)	2.36(− 9)	2.05(− 9)	1.79(− 9)	1.59(− 9)	1.49(− 9)
^{35}Cl	5.56(− 5)	9.16(− 4)	9.15(− 4)	7.54(− 4)	6.23(− 4)	4.97(− 4)	3.94(− 4)	3.09(− 4)	2.47(− 4)	1.97(− 4)	1.68(− 4)	1.48(− 4)	1.41(− 4)	1.55(− 4)
^{37}Cl	1.05(− 7)	5.59(− 4)	6.41(− 4)	6.69(− 4)	6.85(− 4)	6.90(− 4)	6.86(− 4)	6.76(− 4)	6.55(− 4)	6.32(− 4)	6.08(− 4)	5.78(− 4)	5.36(− 4)	4.91(− 4)
^{36}Ar	1.30(− 5)	3.04(− 1)	5.17(− 1)	5.97(− 1)	8.08(− 1)	1.07	1.32	1.54	1.72	1.85	1.94	1.99	1.99	1.93
^{38}Ar	4.89(− 7)	6.26(− 3)	5.28(− 3)	3.39(− 3)	2.23(− 3)	1.41(− 3)	8.96(− 4)	5.57(− 4)	3.56(− 4)	2.22(− 4)	1.48(− 4)	9.78	7.17(− 5)	7.25(− 5)
^{39}K	1.33(− 7)	1.16(− 3)	1.18(− 3)	9.69(− 4)	8.02(− 4)	6.39(− 4)	5.04(− 4)	3.90(− 4)	3.04(− 4)	2.39(− 4)	2.00(− 4)	1.78(− 4)	1.76(− 4)	2.05(− 4)
^{40}K	2.51(−10)	3.49(− 8)	3.02(− 8)	2.19(− 8)	1.69(− 8)	1.28(− 8)	9.67(− 9)	7.29(− 9)	5.46(− 9)	4.05(− 9)	3.17(− 9)	2.54(− 9)	2.27(− 9)	2.60(− 9)
^{41}K	2.45(−10)	1.24(− 4)	1.39(− 4)	1.45(− 4)	1.48(− 4)	1.48(− 4)	1.47(− 4)	1.44(− 4)	1.39(− 4)	1.33(− 4)	1.28(− 4)	1.22(− 4)	1.14(− 4)	1.06(− 4)
^{40}Ca ...	1.46(− 8)	1.88(− 1)	3.17(− 1)	3.70(− 1)	5.29(− 1)	7.61(− 1)	9.93(− 1)	1.22	1.40	1.54	1.63	1.69	1.71	1.67
^{42}Ca ...	2.39(−10)	1.69(− 4)	1.39(− 4)	8.72(− 5)	5.74(− 5)	3.67(− 5)	2.35(− 5)	1.50(− 5)	9.87(− 6)	6.42(− 6)	4.53(− 6)	3.39(− 6)	3.06(− 6)	3.79(− 6)
^{43}Ca ...	3.56(−11)	5.74(− 8)	4.23(− 8)	2.73(− 8)	1.94(− 8)	1.37(− 8)	1.00(− 8)	7.48(− 9)	1.29(− 8)	8.33(− 8)	2.55(− 7)	5.85(− 7)	1.20(− 6)	2.19(− 6)
^{44}Ca ...	6.96(−11)	3.82(− 5)	6.67(− 5)	7.81(− 5)	1.22(− 4)	1.99(− 4)	2.85(− 4)	3.76(− 4)	4.58(− 4)	5.65(− 4)	7.05(− 4)	9.06(− 4)	1.21(− 3)	1.61(− 3)
^{45}Sc	1.40(−11)	2.50(− 6)	2.90(− 6)	3.03(− 6)	3.20(− 6)	3.36(− 6)	3.48(− 6)	3.57(− 6)	3.59(− 6)	3.59(− 6)	3.57(− 6)	3.51(− 6)	3.42(− 6)	3.33(− 6)
^{46}Ti	2.29(−11)	7.36(− 5)	6.75(− 5)	4.68(− 5)	3.39(− 5)	2.49(− 5)	1.86(− 5)	1.41(− 5)	1.10(− 5)	8.54(− 6)	6.86(− 6)	5.36(− 6)	4.01(− 6)	3.03(− 6)
^{47}Ti	5.08(−12)	3.02(− 7)	3.99(− 7)	3.24(− 7)	4.00(− 7)	5.35(− 7)	6.61(− 7)	7.77(− 7)	8.66(− 7)	1.24(− 6)	2.05(− 6)	3.56(− 6)	6.27(− 6)	1.06(− 5)
^{48}Ti	6.41(−12)	5.48(− 5)	4.50(− 4)	5.71(− 4)	1.46(− 3)	3.45(− 3)	6.06(− 3)	9.04(− 3)	1.14(− 2)	1.35(− 2)	1.52(− 2)	1.69(− 2)	1.85(− 2)	2.00(− 2)
^{49}Ti	5.16(−12)	7.62(− 6)	3.05(− 5)	3.37(− 5)	6.25(− 5)	1.15(− 4)	1.80(− 4)	2.54(− 4)	3.05(− 4)	3.44(− 4)	3.71(− 4)	3.90(− 4)	4.01(− 4)	4.00(− 4)
^{51}V	1.10(−12)	1.74(− 5)	6.49(− 5)	6.54(− 5)	1.11(− 4)	1.92(− 4)	2.95(− 4)	4.17(− 4)	4.76(− 4)	5.04(− 4)	5.15(− 4)	5.16(− 4)	5.09(− 4)	4.95(− 4)
^{50}Cr	2.35(−13)	3.15(− 4)	4.65(− 4)	3.84(− 4)	3.99(− 4)	4.34(− 4)	4.87(− 4)	5.65(− 4)	5.68(− 4)	5.42(− 4)	5.15(− 4)	4.85(− 4)	4.51(− 4)	4.20(− 4)
^{52}Cr	1.16(−12)	7.01(− 4)	6.16(− 3)	7.76(− 3)	2.24(− 2)	6.24(− 2)	1.25(− 1)	2.06(− 1)	2.67(− 1)	3.16(− 1)	3.52(− 1)	3.79(− 1)	3.97(− 1)	4.00(− 1)
^{53}Cr	1.60(−13)	1.23(− 4)	5.75(− 4)	6.36(− 4)	1.32(− 3)	2.84(− 3)	5.14(− 3)	8.34(− 3)	1.04(− 2)	1.19(− 2)	1.29(− 2)	1.36(− 2)	1.40(− 2)	1.40(− 2)
^{54}Cr	4.63(−13)	1.90(− 8)	1.75(− 8)	1.13(− 8)	7.36(− 9)	5.23(− 9)	4.31(− 9)	4.19(− 9)	3.54(− 9)	2.84(− 9)	2.33(− 9)	1.91(− 9)	1.58(− 9)	1.31(− 9)
^{55}Mn ...	8.31(−14)	7.02(− 4)	2.75(− 3)	2.91(− 3)	5.43(− 3)	1.11(− 2)	2.02(− 2)	3.49(− 2)	4.26(− 2)	4.63(− 2)	4.82(− 2)	4.85(− 2)	4.85(− 2)	4.75(− 2)

TABLE 3—*Continued*

Ion	65	70	75	80	85	90	95	100	105	110	115	120	125	130
^{54}Fe ...	3.37(−15)	2.46(− 2)	4.49(− 2)	4.06(− 2)	4.94(− 2)	6.44(− 2)	8.79(− 2)	1.30(− 1)	1.42(− 1)	1.41(− 1)	1.38(− 1)	1.31(− 1)	1.24(− 1)	1.18(− 1)
^{56}Fe ...	1.31(−13)	1.17(− 2)	1.02(− 1)	1.29(− 1)	4.07(− 1)	1.31	2.98	5.82	9.55	1.42(1)	1.90(1)	2.46(1)	3.17(1)	3.96(1)
^{57}Fe ...	2.80(−14)	2.40(− 4)	1.08(− 3)	1.21(− 3)	2.63(− 3)	6.37(− 3)	1.33(− 2)	2.77(− 2)	6.97(− 2)	1.41(− 1)	2.26(− 1)	3.39(− 1)	5.04(− 1)	7.16(− 1)
^{58}Fe ...	5.78(−14)	1.08(− 8)	1.12(− 8)	9.34(− 9)	8.04(− 9)	7.18(− 9)	6.47(− 9)	6.05(− 9)	5.35(− 9)	4.41(− 9)	3.72(− 9)	2.94(− 9)	2.32(− 9)	1.88(− 9)
^{59}Co ...	1.56(−14)	3.67(− 6)	4.09(− 6)	4.34(− 6)	4.60(− 6)	5.05(− 6)	5.59(− 6)	1.31(− 5)	6.67(− 4)	2.28(− 3)	4.47(− 3)	7.62(− 3)	1.25(− 2)	1.93(− 2)
^{58}Ni ...	6.40(−17)	1.34(− 3)	2.48(− 3)	2.46(− 3)	3.36(− 3)	5.11(− 3)	8.24(− 3)	1.84(− 2)	8.66(− 2)	2.07(− 1)	3.59(− 1)	5.77(− 1)	9.30(− 1)	1.47
^{60}Ni ...	1.58(−14)	7.16(− 6)	7.18(− 6)	6.73(− 6)	6.24(− 6)	5.94(− 6)	5.55(− 6)	3.69(− 5)	9.03(− 3)	3.67(− 2)	7.61(− 2)	1.32(− 1)	2.13(− 1)	3.13(− 1)
^{61}Ni ...	4.68(−15)	8.05(−10)	8.87(−10)	9.11(−10)	9.40(−10)	9.90(−10)	1.04(− 9)	1.91(− 6)	5.42(− 4)	2.22(− 3)	4.60(− 3)	7.99(− 3)	1.29(− 2)	1.92(− 2)
^{62}Ni ...	2.05(−14)	1.47(−10)	2.18(−10)	1.97(−10)	2.45(−10)	3.62(−10)	6.33(−10)	7.97(− 6)	2.65(− 3)	1.15(− 2)	2.51(− 2)	4.59(− 2)	8.04(− 2)	1.33(− 1)
^{63}Cu ...	2.55(−15)	3.92(−12)	4.33(−12)	4.78(−12)	5.04(−12)	5.55(−12)	6.41(−12)	2.90(− 9)	1.49(− 6)	7.14(− 6)	1.62(− 5)	3.04(− 5)	5.39(− 5)	8.93(− 5)
^{65}Cu ...	3.35(−15)	8.19(−15)	1.01(−14)	1.75(−14)	1.89(−14)	1.80(−14)	1.48(−14)	3.06(−10)	7.71(− 7)	4.47(− 6)	1.07(− 5)	2.04(− 5)	3.53(− 5)	5.50(− 5)
^{64}Zn ...	1.39(−15)	1.68(−11)	1.93(−11)	2.32(−11)	2.58(−11)	2.74(−11)	2.86(−11)	4.22(− 9)	8.97(− 6)	5.11(− 5)	1.21(− 4)	2.29(− 4)	3.93(− 4)	6.00(− 4)
^{66}Zn ...	3.22(−15)	8.57(−15)	1.08(−14)	2.28(−14)	2.23(−14)	1.71(−14)	8.52(−15)	5.50(− 9)	1.40(− 5)	8.43(− 5)	2.07(− 4)	4.09(− 4)	7.52(− 4)	1.28(− 3)
^{67}Zn ...	6.27(−16)	4.18(−16)	4.13(−16)	4.69(−16)	3.13(−16)	4.92(−16)	6.63(−17)	3.86(−12)	1.13(− 8)	7.11(− 8)	1.80(− 7)	3.63(− 7)	6.85(− 7)	1.20(− 6)
^{68}Zn ...	3.58(−15)	1.85(−15)	1.80(−15)	2.02(−15)	1.26(−15)	2.18(−15)	2.72(−16)	9.36(−13)	3.31(− 9)	2.30(− 8)	6.12(− 8)	1.29(− 7)	2.58(− 7)	4.82(− 7)
^{69}Ga ...	4.96(−16)	4.19(−16)	3.86(−16)	4.20(−16)	2.29(−16)	4.07(−16)	2.60(−17)	2.72(−14)	3.41(−10)	2.63(− 9)	7.11(− 9)	1.47(− 8)	2.75(− 8)	4.58(− 8)
^{71}Ga ...	4.53(−16)	2.19(−16)	2.00(−16)	2.19(−16)	1.15(−16)	2.06(−16)	1.15(−17)	8.19(−15)	2.34(−10)	2.00(− 9)	5.59(− 9)	1.18(− 8)	2.27(− 8)	3.94(− 8)
^{70}Ge ...	6.63(−16)	1.33(−15)	1.43(−15)	1.61(−15)	9.13(−16)	1.70(−15)	1.08(−16)	4.04(−12)	9.27(− 8)	7.68(− 7)	2.12(− 6)	4.43(− 6)	8.46(− 6)	1.46(− 5)
^{72}Ge ...	7.04(−16)	4.76(−16)	4.11(−16)	4.36(−16)	2.17(−16)	3.87(−16)	2.04(−17)	3.35(−15)	1.85(−10)	1.79(− 9)	5.37(− 9)	1.20(− 8)	2.50(− 8)	4.81(− 8)
^{74}Se ...	2.74(−19)	2.34(−16)	3.16(−16)	3.83(−16)	2.24(−16)	4.61(−16)	2.49(−17)	6.27(−16)	2.18(−10)	2.54(− 9)	7.86(− 9)	1.74(− 8)	3.37(− 8)	5.75(− 8)

NOTE.—Table 3 is also available in machine-readable form in the electronic edition of the *Astrophysical Journal*.

was already composed of more than 50% oxygen-burning products, chiefly silicon and sulfur, and the mass fraction of iron in the stellar center was 0.1 (^{54}Fe).

Eight days later, a third and final violent pulse occurred, powered again by off-center explosive oxygen burning. This pulse went to a central temperature of 4.5×10^9 K and density 2.0×10^6 g cm^{-3} and was more violent than the second (but less than the first). It ejected 2.2 $M_\odot$ with kinetic energy 5.1×10^{50} ergs. The expansion also was more extreme, central conditions declining to the point (8.5×10^8 K; 1.9×10^5 g cm^{-3}) where neutrino losses were not very efficient (although still greater than the surface luminosity by orders of magnitude). At this point the oxygen-depleted core was 5 $M_\odot$, and the inner 0.8 $M_\odot$ of the star was mostly iron.

The final contraction phase followed lasted 1.8 yr. The stellar core then settled into stable silicon shell burning with no more pair instability pulses. Silicon burned in a series of shells, each encompassing about 0.2 $M_\odot$ (zoning was 0.01 $M_\odot$) until the iron core grew to 1.8 $M_\odot$ and collapsed on the photodisintegration instability. It should be noted, however, that this collapsing core differed in a variety of ways from those found in lower mass stars: (1) There was no steep decline in density around the iron core nor a sharp increase in entropy usually associated with the oxygen-burning shell. The oxygen shell was, in fact, at $m = 5.3\ M_\odot$. (2) The entropy (in units of k_B baryon^{-1}) in the core and its surrounding were anomalously large, ranging from 1 at the center to 3 at the edge of the iron core and 6.0 at $m = 3\ M_\odot$. (3) The central electron mole number, $Y_e = 0.446$, was unusually large and the value in the outer core, larger still, 0.490. (4) The net binding energy outside the iron core was -3.9×10^{51} ergs. All these differences go in the direction of a less centrally condensed structure that will be harder to explode (Wilson et al. 1986; Fryer 1999). We believe that, in the absence of very appreciable rotation, this star will become a black hole.

A similar behavior was observed for the 45 $M_\odot$ helium core of a 100 $M_\odot$ main-sequence star studied by Woosley (1986). That star experienced four pulses resulting from the pair instability before settling down to burn silicon stably and also become a black hole (Wilson et al. 1986). The pulses were less violent, although with a total duration of only 1.6 yr. This probably marks the lower extremity of the pulsational pair domain, but stars in between might have intermediate energies and durations. The relevance of such objects, e.g., SN 1961V (see, e.g., Filippenko et al. 1995) and η Carinae (Davidson et al. 1999), remains largely unexplored. Lacking radioactivity, the ejecta might not be bright, but this would be greatly altered if the explosion occurred inside a star that still had an extended hydrogen envelope or when the ejected shells ran into one another.

On the upper boundary of the mass range for pair instability, violent explosions are found that leave no bound remnant. A 133.3 $M_\odot$ helium core exploded with a kinetic energy of 93.5×10^{51} ergs and ejected 57.0 $M_\odot$ of ^{56}Ni. This is approximately 100 times the ^{56}Ni produced by a typical Type Ia supernova and, for a bare helium star, might have a peak luminosity 100 times as great (i.e., $\sim 10^{45}$ ergs s^{-1}). Even inside a blue supergiant, as one might expect for Population III stars at death, the radioactive display would be spectacular, brighter than a galaxy. The explosion would be the most energetic thermonuclear explosion in the universe. At the point of highest density (1.9×10^7 g cm^{-3}) in this model, a central temperature of 7.4×10^9 K is reached, and the star contains 19.4 $M_\odot$ of ^{4}He, 0.98 $M_\odot$ of protons, and 0.054 $M_\odot$ of neutrons from photodisintegration, corresponding to about 5×10^{52} ergs that is released when they recombine to ^{56}Ni. During the collapse phase the helium-rich layer collapses rapidly onto the helium-free core, and helium is burned implosively even up to silicon as the dominant product.

However, going just a small step up in mass, for a non-rotating star, gives no explosion at all. For a 133.31 $M_\odot$ helium star, the infall did not turn around into an explosion but instead continued, after a brief phase of slowing, into a black hole. With rotation, the evolution of all these stars could be greatly altered (Glatzel et al. 1985; Stringfellow & Woosley 1988; Fryer et al. 2001).

Immediately below the *lower* boundary of the mass range for pair instability supernovae, it is also likely that black holes are the main product. This is because either a successful outgoing shock fails to be launched for stars above about 40 $M_\odot$ (Fryer 1999) or the shock is so weak that fallback converts the neutron star into a black hole. Either way the star fails to eject most of its heavy elements. Woosely & Weaver (1995) find, for an assumed constant explosion energy of about 1.2×10^{51} ergs, that the final collapsed remnant in Population III stars of masses 22, 25, 30, 35, and 40 $M_\odot$ are 1.5, 6.4, 8.2, 13, and 17 $M_\odot$, respectively. Apparently, above about 30 $M_\odot$ the heavy-element synthesis of ordinary Population III supernovae (i.e., not pair-unstable) is negligible.

The fact that the pair supernova domain is bounded above and below by stars that make black holes (Fig. 2) and the fact that the explosion is easy to calculate make the nucleosynthesis from this mass range easy to determine unambiguously provided one specifies an IMF.

3.2. *Nucleosynthetic Results*

The yields for all the models are given in Table 3 for each stable nucleus created in any appreciable abundance compared with the Sun. Values are given in solar masses after all unstable progenitors have decayed. The value given for ^{56}Fe, in particular, is actually that of ^{56}Ni. The reaction network included sufficient weak interactions to follow accurately the evolving neutron excess. Final central values for the central value of η for our fiducial helium stars of 80, 100, and 120 $M_\odot$ are 0.00034, 0.0016 and 0.0037, respectively. Even for 130 $M_\odot$, the value was 0.0052. As one moves out from the center, the neutron excess declines rapidly. These small values ensure that ^{56}Fe and other abundant nuclei like ^{48}Ti, ^{52}Cr, and ^{60}Ni are made as their $Z = N$ progenitors. In the last column of Table 2 the central neutron excess η_c is given at the time of maximum density of the star.

Table 4 gives the production factors corresponding to these yields. The production factor P_i is defined as the ratio of the mass fraction of a given species in the ejecta compared to its mass fraction in the Sun. One implication is that "solar production" of a given isotope could occur in a star having a metallicity of, say, $[Z] = -3$ (0.1% that of the Sun) if a fraction, $10^{-3}/P_i$, of that star's mass had passed through pair instability supernovae of the given type. Of course, one must normalize to the greatest P_i, and all species having smaller P_i would be underproduced relative to the Sun.

Already obvious in Tables 3 and 4 is the small production of nuclei that require excess neutrons for their existence.

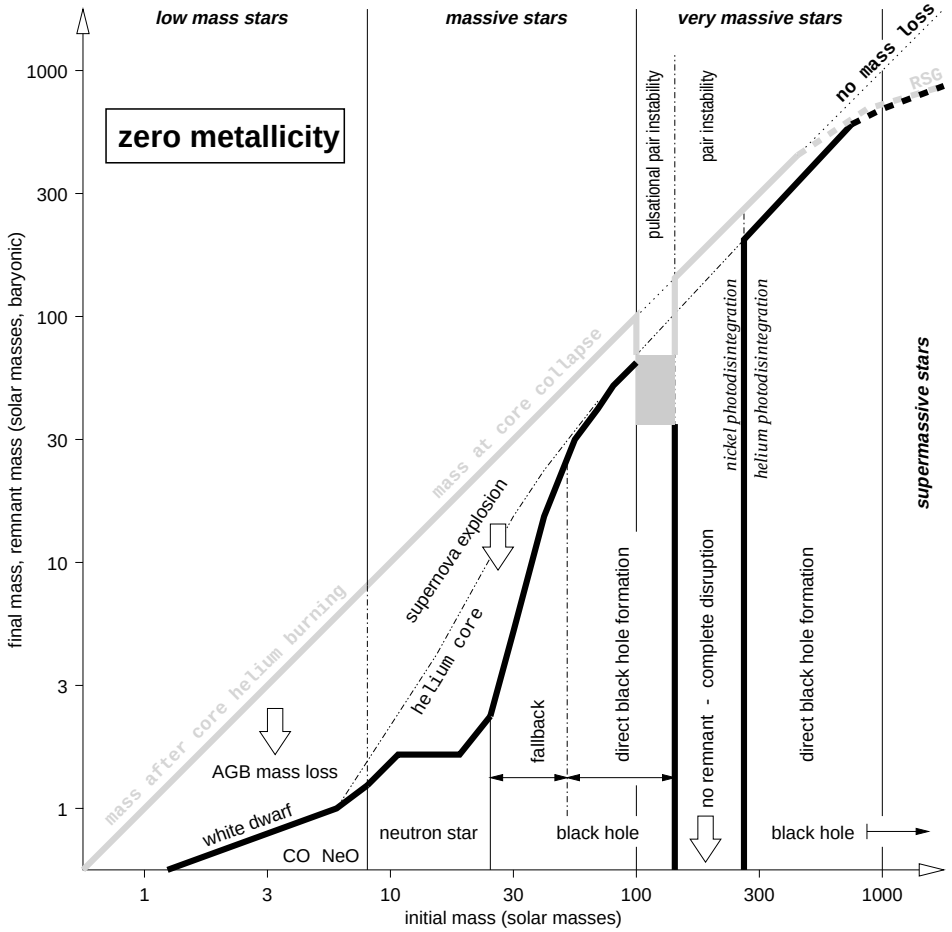

FIG. 2.—Initial-final mass function of nonrotating primordial stars ($Z = 0$). The x-axis gives the initial stellar mass. The y-axis gives both the final mass of the collapsed remnant (*thick black curve*) and the mass of the star when the event begins that produces that remnant (e.g., mass loss in AGB stars, supernova explosion for those stars that make a neutron star, etc.; *thick gray curve*). We distinguish four regimes of initial mass: low-mass stars below $\sim 10\ M_\odot$ that end as white dwarfs; massive stars between ~ 10 and $\sim 100\ M_\odot$; very massive stars between ~ 100 and $\sim 1000\ M_\odot$; and supermassive stars (arbitrarily) above $\sim 1000\ M_\odot$. Since no mass loss is expected for $Z = 0$ stars before the final stage, the gray curve is approximately the same as the line of no mass loss (*dotted line*). Exceptions are ~ 100–$140\ M_\odot$, where the pulsational pair instability ejects the outer layers of the star before it collapses, and above $\sim 500\ M_\odot$, where pulsational instabilities in red supergiants may lead to significant mass loss (Baraffe et al. 2001). Since the magnitude of the latter is uncertain, lines are dashed. In the low-mass regime we assume, even in $Z = 0$ stars, that mass loss on the AGB leads to the star losing its envelope and becoming a CO or NeO white dwarf (although the mechanism and thus the resulting initial-final mass function may differ from solar composition stars). "Massive stars" are defined as stars that ignite carbon and oxygen burning nondegenerately and do not leave white dwarfs. The hydrogen-rich envelope and parts of the helium core (*dashed–double-dotted curve*) are ejected in a supernova explosion. Below an initial mass of $\sim 25\ M_\odot$, neutron stars are formed. Above that, black holes form, either in a delayed manner by fallback of the ejecta or directly during iron core collapse (above $\sim 40\ M_\odot$). The defining characteristic of *very* massive stars is the electron-positron *pair instability* after carbon burning. This begins as a pulsational instability for helium cores of $\sim 40\ M_\odot$ ($M_{\rm ZAMS} \sim 100\ M_\odot$). As the mass increases, the pulsations become more violent, ejecting any remaining hydrogen envelope and an increasing fraction of the helium core itself. An iron core can still eventually form in hydrostatic equilibrium in such stars, but it collapses to a black hole. Above $M_{\rm He} = 63\ M_\odot$ or about $M_{\rm ZAMS} = 140\ M_\odot$, and on up to $M_{\rm He} = 133\ M_\odot$ or about $M_{\rm ZAMS} = 260\ M_\odot$, a single pulse disrupts the star. Above $260\ M_\odot$, the pair instability in nonrotating stars results in complete collapse to a black hole.

This includes all nuclei with odd charge above ^{14}N: ^{23}Na, ^{27}Al, ^{31}P, and the like—as well as neutron-rich isotopes like ^{29,30}Si, ^{33,34,36}S, ^{38}Ar, etc. Such nuclei all require a neutron excess for their production. They are underproduced here because of the low value of η in all regions of all stars except the deep interiors of the most massive explosions (thus, ^{54}Fe has an appreciable yield in the $130\ M_\odot$ model). Also absent is any appreciable nucleosynthesis for $A \gtrsim 66$.

Elements above the iron group are absent because there was no s- or r-process in our stars. The r-process requires very rapid expansion timescales from extremely high temperature, high entropy, and a large neutron excess. None of these are realized here. The s-process requires a neutron source—such as ^{22}Ne$(\alpha, n)^{25}$Mg or ^{13}C$(\alpha, n)^{16}$O—and heavy-element "seed nuclei." There are no seed nuclei in our Population III stars, and very little ^{13}C or ^{22}Ne is present during helium burning. (Since we studied helium stars, any possible production of ^{13}C that might result from the interpenetration of hydrogen envelope and convective helium shell was not followed. This has never been demonstrated to give neutrons in a massive star but might be worth further investigation.)

The neutron excess is low in our stars because (1) the assumed Population III initial helium core composition (Table 1) implies a very small value of η at the end of helium burning. This η comes about from the conversion of ^{14}N into ^{18}O early in helium burning by ^{14}N$(\alpha, \gamma)^{18}$F$(e^+, \nu)^{18}$O. The abundance of CNO is very low in Population III stars). (2) Subsequent burning stages occur too rapidly and at too

TABLE 4

PRODUCTION FACTORS (RELATIVE TO SOLAR)

Ion	65	70	75	80	85	90	95	100	105	110	115	120	125	130
^{4}He	1.10(− 1)	8.05(− 2)	6.97(− 2)	6.61(− 2)	6.15(− 2)	5.70(− 2)	5.45(− 2)	5.33(− 2)	5.28(− 2)	5.48(− 2)	5.61(− 2)	6.04(− 2)	6.91(− 2)	7.89(− 2)
^{11}B	2.38(− 7)	2.35(− 8)	8.04(− 7)	1.79(− 6)	3.55(− 6)	5.29(− 6)	6.87(− 6)	8.42(− 6)	9.73(− 6)	1.08(− 5)	1.18(− 5)	1.23(− 5)	1.26(− 5)	1.24(− 5)
^{12}C	3.50(1)	2.14(1)	1.90(1)	1.79(1)	1.66(1)	1.54(1)	1.43(1)	1.32(1)	1.21(1)	1.12(1)	1.07(1)	1.02(1)	9.53	8.85
^{13}C	9.84(− 5)	1.64(− 4)	2.72(− 4)	3.04(− 4)	2.74(− 4)	1.76(− 4)	1.03(− 4)	1.18(− 4)	6.00(− 5)	3.98(− 5)	3.91(− 5)	3.45(− 5)	3.03(− 5)	1.97(− 5)
^{14}N	1.09(− 3)	6.51(− 4)	5.20(− 4)	4.70(− 4)	4.03(− 4)	3.48(− 4)	3.07(− 4)	2.80(− 4)	2.52(− 4)	2.26(− 4)	1.91(− 4)	1.47(− 4)	1.02(− 4)	7.65(− 5)
^{15}N	2.56(− 3)	2.30(− 2)	2.05(− 2)	1.92(− 2)	1.77(− 2)	1.64(− 2)	1.55(− 2)	1.47(− 2)	1.42(− 2)	1.41(− 2)	1.39(− 2)	1.37(− 2)	1.29(− 2)	1.17(− 2)
^{16}O	7.90(1)	6.83(1)	6.18(1)	6.10(1)	5.72(1)	5.32(1)	4.96(1)	4.58(1)	4.24(1)	3.90(1)	3.60(1)	3.31(1)	2.99(1)	2.68(1)
^{17}O	1.69(− 2)	3.62(− 3)	2.66(− 3)	2.40(− 3)	2.00(− 3)	1.70(− 3)	1.46(− 3)	1.31(− 3)	1.16(− 3)	1.04(− 3)	9.24(− 4)	8.02(− 4)	6.70(− 4)	5.66(− 4)
^{18}O	1.99(− 3)	6.55(− 4)	5.23(− 4)	4.70(− 4)	4.32(− 4)	4.02(− 4)	3.71(− 4)	3.74(− 4)	3.51(− 4)	3.45(− 4)	3.35(− 4)	3.27(− 4)	3.28(− 4)	3.01(− 4)
^{19}F	6.20(− 4)	4.96(− 4)	4.23(− 4)	3.79(− 4)	3.59(− 4)	3.90(− 4)	4.18(− 4)	4.17(− 4)	4.54(− 4)	4.56(− 4)	5.15(− 4)	5.40(− 4)	5.46(− 4)	4.89(− 4)
^{20}Ne ...	4.75(1)	3.56(1)	3.20(1)	3.26(1)	3.06(1)	2.82(1)	2.59(1)	2.51(1)	2.27(1)	2.19(1)	2.06(1)	2.00(1)	1.94(1)	1.77(1)
^{21}Ne ...	1.88	2.26(− 1)	6.78(− 1)	7.55(− 1)	8.53(− 1)	6.77(− 1)	4.64(− 1)	5.18(− 1)	3.28(− 1)	3.64(− 1)	3.06(− 1)	3.07(− 1)	3.26(− 1)	2.32(− 1)
^{22}Ne ...	2.20(− 2)	2.20(− 3)	1.90(− 3)	1.89(− 3)	1.98(− 3)	1.94(− 3)	1.83(− 3)	1.82(− 3)	1.67(− 3)	1.72(− 3)	1.60(− 3)	1.54(− 3)	1.43(− 3)	1.19(− 3)
^{23}Na ...	4.21	1.34	1.18	1.13	1.04	9.58(− 1)	8.88(− 1)	8.27(− 1)	7.69(− 1)	7.26(− 1)	6.97(− 1)	6.85(− 1)	6.72(− 1)	6.41(− 1)
^{24}Mg...	4.57(1)	8.38(1)	9.03(1)	8.92(1)	9.08(1)	9.16(1)	8.95(1)	8.57(1)	8.15(1)	7.61(1)	7.60(1)	7.37(1)	6.87(1)	6.54(1)
^{25}Mg...	8.61(− 1)	2.28(− 1)	6.06(− 1)	4.12(− 1)	5.85(− 1)	6.81(− 1)	7.32(− 1)	6.32(− 1)	6.43(− 1)	6.11(− 1)	5.19(− 1)	4.63(− 1)	4.01(− 1)	4.05(− 1)
^{26}Mg...	7.36(− 1)	3.20(− 1)	2.90(− 1)	2.80(− 1)	2.72(− 1)	2.75(− 1)	2.80(− 1)	2.47(− 1)	2.52(− 1)	2.23(− 1)	2.17(− 1)	2.00(− 1)	1.77(− 1)	1.71(− 1)
^{27}Al	8.95	4.36	3.82	3.43	3.39	3.30	3.21	2.81	2.73	2.42	2.25	2.03	1.78	1.78
^{28}Si	7.43	1.74(2)	2.50(2)	2.60(2)	2.97(2)	3.27(2)	3.45(2)	3.53(2)	3.57(2)	3.51(2)	3.42(2)	3.28(2)	3.08(2)	2.85(2)
^{29}Si	8.80(− 1)	9.69	8.74	8.11	7.35	6.72	6.30	5.67	5.39	4.80	4.52	4.09	3.55	3.35
^{30}Si	4.27	1.66	8.36(− 1)	7.07(− 1)	6.16(− 1)	5.81(− 1)	6.07(− 1)	5.08(− 1)	5.88(− 1)	5.24(− 1)	5.30(− 1)	4.87(− 1)	3.99(− 1)	4.40(− 1)
^{31}P	5.12	5.07	3.54	2.90	2.37	1.98	1.75	1.46	1.44	1.21	1.25	1.14	9.36(− 1)	1.01
^{32}S	3.69(− 2)	8.77(1)	1.39(2)	1.48(2)	1.81(2)	2.13(2)	2.36(2)	2.52(2)	2.61(2)	2.63(2)	2.59(2)	2.52(2)	2.40(2)	2.22(2)
^{33}S	1.84(− 1)	1.36(1)	1.45(1)	1.41(1)	1.36(1)	1.29(1)	1.22(1)	1.14(1)	1.06(1)	9.78	9.03	8.24	7.36	6.47
^{34}S	1.70(− 1)	4.87	3.27	1.97	1.21	7.27(− 1)	4.42(− 1)	2.67(− 1)	1.68(− 1)	1.03(− 1)	6.94(− 2)	4.82(− 2)	3.79(− 2)	4.03(− 2)
^{36}S	1.84(− 3)	1.70(− 3)	1.12(− 3)	8.80(− 4)	6.95(− 4)	5.39(− 4)	4.29(− 4)	3.45(− 4)	2.78(− 4)	2.29(− 4)	1.90(− 4)	1.60(− 4)	1.35(− 4)	1.22(− 4)
^{35}Cl	3.38(− 1)	5.17	4.82	3.73	2.90	2.18	1.64	1.22	9.29(− 1)	7.09(− 1)	5.77(− 1)	4.87(− 1)	4.45(− 1)	4.72(− 1)
^{37}Cl	1.88(− 3)	9.35	1.00(1)	9.79	9.44	8.98	8.45	7.91	7.31	6.73	6.19	5.64	5.03	4.42
^{36}Ar	2.59(− 3)	5.62(1)	8.92(1)	9.64(1)	1.23(2)	1.54(2)	1.79(2)	1.99(2)	2.11(2)	2.17(2)	2.18(2)	2.14(2)	2.05(2)	1.92(2)
^{38}Ar	4.90(− 4)	5.82	4.58	2.76	1.71	1.02	6.13(− 1)	3.62(− 1)	2.21(− 1)	1.31(− 1)	8.34(− 2)	5.30(− 2)	3.73(− 2)	3.63(− 2)
^{40}Ar	4.64(− 5)	3.84(− 5)	2.30(− 5)	1.71(− 5)	1.57(− 5)	1.21(− 5)	1.20(− 5)	1.18(− 5)	8.77(− 6)	8.30(− 6)	1.12(− 5)	1.06(− 5)	1.31(− 5)	1.74(− 5)
^{39}K	5.89(− 4)	4.77	4.52	3.49	2.72	2.05	1.53	1.12	8.36(− 1)	6.26(− 1)	5.02(− 1)	4.26(− 1)	4.05(− 1)	4.55(− 1)
^{40}K	6.96(− 4)	8.99(− 2)	7.27(− 2)	4.93(− 2)	3.60(− 2)	2.56(− 2)	1.84(− 2)	1.32(− 2)	9.38(− 3)	6.65(− 3)	4.97(− 3)	3.81(− 3)	3.28(− 3)	3.61(− 3)
^{41}K	1.43(− 5)	6.72	7.05	6.88	6.60	6.26	5.87	5.47	5.02	4.61	4.23	3.85	3.46	3.09
^{40}Ca ...	3.75(− 6)	4.48(1)	7.06(1)	7.72(1)	1.04(2)	1.41(2)	1.74(2)	2.03(2)	2.22(2)	2.33(2)	2.37(2)	2.36(2)	2.29(2)	2.15(2)
^{42}Ca ...	8.77(− 6)	5.75	4.42	2.60	1.61	9.72(− 1)	5.91(− 1)	3.59(− 1)	2.24(− 1)	1.39(− 1)	9.40(− 2)	6.74(− 2)	5.85(− 2)	6.94(− 2)
^{43}Ca ...	6.11(− 6)	9.15(− 3)	6.29(− 3)	3.80(− 3)	2.54(− 3)	1.70(− 3)	1.18(− 3)	8.34(− 4)	1.37(− 3)	8.45(− 3)	2.47(− 2)	5.43(− 2)	1.07(− 1)	1.88(− 1)
^{44}Ca ...	7.52(− 7)	3.83(− 1)	6.24(− 1)	6.85(− 1)	1.00	1.55	2.10	2.64	3.06	3.61	4.30	5.30	6.79	8.67
^{46}Ca ...	3.11(− 7)	5.30(− 8)	4.66(− 9)	2.95(− 9)	2.01(− 9)	1.40(− 9)	7.63(−10)	5.98(−10)	8.11(−10)	7.43(−10)	3.79(−10)	3.99(−10)	3.50(−10)	3.35(−10)
^{45}Sc	5.55(− 6)	9.19(− 1)	9.93(− 1)	9.74(− 1)	9.67(− 1)	9.60(− 1)	9.40(− 1)	9.18(− 1)	8.79(− 1)	8.38(− 1)	7.97(− 1)	7.53(− 1)	7.04(− 1)	6.59(− 1)
^{46}Ti	1.58(− 6)	4.71	4.03	2.62	1.79	1.24	8.75(− 1)	6.33(− 1)	4.69(− 1)	3.48(− 1)	2.67(− 1)	2.00(− 1)	1.44(− 1)	1.04(− 1)
^{47}Ti	3.76(− 7)	2.08(− 2)	2.56(− 2)	1.94(− 2)	2.26(− 2)	2.85(− 2)	3.35(− 2)	3.74(− 2)	3.96(− 2)	5.42(− 2)	8.58(− 2)	1.42(− 1)	2.41(− 1)	3.90(− 1)
^{48}Ti	4.59(− 8)	3.65(− 1)	2.80	3.32	7.97	1.78(1)	2.97(1)	4.21(1)	5.06(1)	5.71(1)	6.17(1)	6.55(1)	6.90(1)	7.15(1)
^{49}Ti	4.85(− 7)	6.65(− 1)	2.49	2.58	4.49	7.82	1.16(1)	1.55(1)	1.78(1)	1.91(1)	1.97(1)	1.99(1)	1.96(1)	1.88(1)
^{50}Ti	6.43(− 7)	3.53(− 7)	2.02(− 7)	1.82(− 7)	1.33(− 7)	1.39(− 7)	5.71(− 8)	3.95(− 8)	1.01(− 7)	9.07(− 8)	2.29(− 8)	4.34(− 8)	3.61(− 8)	2.28(− 8)
^{50}V	6.42(− 6)	3.08(− 3)	1.95(− 3)	9.64(− 4)	5.40(− 4)	3.15(− 4)	1.98(− 4)	1.34(− 4)	9.30(− 5)	6.29(− 5)	4.38(− 5)	3.12(− 5)	2.20(− 5)	1.65(− 5)
^{51}V	4.48(− 8)	6.58(− 1)	2.30	2.17	3.45	5.67	8.24	1.11(1)	1.20(1)	1.22(1)	1.19(1)	1.14(1)	1.08(1)	1.01(1)
^{50}Cr	4.87(− 9)	6.06	8.35	6.47	6.32	6.50	6.91	7.61	7.29	6.64	6.04	5.44	4.86	4.36

TABLE 4—*Continued*

Ion	65	70	75	80	85	90	95	100	105	110	115	120	125	130
^{52}Cr	1.20(− 9)	6.74(− 1)	5.53	6.53	1.77(1)	4.67(1)	8.83(1)	1.39(2)	1.71(2)	1.94(2)	2.06(2)	2.13(2)	2.14(2)	2.07(2)
^{53}Cr	1.44(− 9)	1.02	4.47	4.63	9.03	1.84(1)	3.15(1)	4.86(1)	5.79(1)	6.30(1)	6.54(1)	6.61(1)	6.54(1)	6.29(1)
^{54}Cr	1.64(− 8)	6.22(− 4)	5.34(− 4)	3.25(− 4)	1.99(− 4)	1.33(− 4)	1.04(− 4)	9.62(− 5)	7.75(− 5)	5.92(− 5)	4.66(− 5)	3.66(− 5)	2.90(− 5)	2.32(− 5)
^{55}Mn...	9.62(−11)	7.55(− 1)	2.76	2.73	4.81	9.25	1.60(1)	2.63(1)	3.05(1)	3.17(1)	3.15(1)	3.04(1)	2.92(1)	2.75(1)
^{54}Fe	7.28(−13)	4.94	8.40	7.12	8.16	1.00(1)	1.30(1)	1.82(1)	1.90(1)	1.80(1)	1.68(1)	1.53(1)	1.39(1)	1.27(1)
^{56}Fe	1.73(−12)	1.43(− 1)	1.16	1.38	4.10	1.24(1)	2.69(1)	4.98(1)	7.79(1)	1.11(2)	1.41(2)	1.75(2)	2.17(2)	2.61(2)
^{57}Fe	1.51(−11)	1.20(− 1)	5.03(− 1)	5.28(− 1)	1.08	2.48	4.91	9.69	2.32(1)	4.48(1)	6.88(1)	9.91(1)	1.41(2)	1.93(2)
^{58}Fe	2.41(−10)	4.18(− 5)	4.03(− 5)	3.16(− 5)	2.56(− 5)	2.16(− 5)	1.84(− 5)	1.64(− 5)	1.38(− 5)	1.08(− 5)	8.75(− 6)	6.62(− 6)	5.02(− 6)	3.92(− 6)
^{59}Co ...	7.14(−11)	1.56(− 2)	1.62(− 2)	1.62(− 2)	1.61(− 2)	1.67(− 2)	1.75(− 2)	3.91(− 2)	1.89	6.18	1.16(1)	1.89(1)	2.98(1)	4.43(1)
^{58}Ni	1.99(−14)	3.88(− 1)	6.70(− 1)	6.22(− 1)	8.00(− 1)	1.15	1.75	3.71	1.67(1)	3.81(1)	6.31(1)	9.72(1)	1.50(2)	2.29(2)
^{60}Ni	1.24(−11)	5.23(− 3)	4.89(− 3)	4.30(− 3)	3.75(− 3)	3.37(− 3)	2.98(− 3)	1.89(− 2)	4.39	1.71(1)	3.38(1)	5.61(1)	8.70(1)	1.23(2)
^{61}Ni	8.39(−11)	1.34(− 5)	1.38(− 5)	1.33(− 5)	1.29(− 5)	1.28(− 5)	1.28(− 5)	2.22(− 2)	6.01	2.35(1)	4.66(1)	7.75(1)	1.21(2)	1.72(2)
^{62}Ni	1.13(−10)	7.56(− 7)	1.05(− 6)	8.89(− 7)	1.04(− 6)	1.45(− 6)	2.40(− 6)	2.87(− 2)	9.11	3.78(1)	7.85(1)	1.38(2)	2.32(2)	3.68(2)
^{63}Cu ...	6.81(−11)	9.74(− 8)	1.00(− 7)	1.04(− 7)	1.03(− 7)	1.07(− 7)	1.17(− 7)	5.04(− 5)	2.47(− 2)	1.13(− 1)	2.44(− 1)	4.40(− 1)	7.51(− 1)	1.20
^{65}Cu ...	1.95(−10)	4.42(−10)	5.09(−10)	8.24(−10)	8.41(−10)	7.55(−10)	5.89(−10)	1.16(− 5)	2.78(− 2)	1.54(− 1)	3.51(− 1)	6.42(− 1)	1.07	1.60
^{64}Zn ...	2.16(−11)	2.43(− 7)	2.59(− 7)	2.92(− 7)	3.06(− 7)	3.07(− 7)	3.03(− 7)	4.25(− 5)	8.62(− 2)	4.68(− 1)	1.06	1.92	3.17	4.66
^{66}Zn ...	8.44(−11)	2.08(−10)	2.46(−10)	4.86(−10)	4.47(−10)	3.23(−10)	1.53(−10)	9.37(− 5)	2.27(− 1)	1.30	3.07	5.80	1.02(1)	1.68(1)
^{67}Zn ...	1.10(−10)	6.82(−11)	6.29(−11)	6.69(−11)	4.20(−11)	6.25(−11)	7.97(−12)	4.41(− 7)	1.23(− 3)	7.38(− 3)	1.79(− 2)	3.45(− 2)	6.26(− 2)	1.06(− 1)
^{68}Zn ...	1.36(−10)	6.52(−11)	5.93(−11)	6.23(−11)	3.65(−11)	5.97(−11)	7.05(−12)	2.31(− 8)	7.78(− 5)	5.15(− 4)	1.31(− 3)	2.65(− 3)	5.08(− 3)	9.13(− 3)
^{69}Ga ...	1.93(−10)	1.51(−10)	1.30(−10)	1.33(−10)	6.79(−11)	1.14(−10)	6.92(−12)	6.86(− 9)	8.21(− 5)	6.03(− 4)	1.56(− 3)	3.10(− 3)	5.56(− 3)	8.89(− 3)
^{71}Ga ...	2.65(−10)	1.19(−10)	1.01(−10)	1.04(−10)	5.13(−11)	8.72(−11)	4.60(−12)	3.12(− 9)	8.49(− 5)	6.93(− 4)	1.85(− 3)	3.75(− 3)	6.91(− 3)	1.15(− 2)
^{70}Ge ...	2.36(−10)	4.40(−10)	4.41(−10)	4.67(−10)	2.49(−10)	4.37(−10)	2.62(−11)	9.36(− 7)	2.04(− 2)	1.62(− 1)	4.26(− 1)	8.56(− 1)	1.57	2.61
^{72}Ge ...	1.82(−10)	1.15(−10)	9.23(−11)	9.18(−11)	4.31(−11)	7.24(−11)	3.61(−12)	5.64(−10)	2.96(− 5)	2.74(− 4)	7.87(− 4)	1.69(− 3)	3.37(− 3)	6.23(− 3)
^{73}Ge ...	1.71(−10)	9.87(−11)	8.91(−11)	9.28(−11)	4.61(−11)	8.08(−11)	4.10(−12)	8.80(−12)	9.81(− 7)	9.82(− 6)	2.80(− 5)	5.85(− 5)	1.07(− 4)	1.69(− 4)
^{75}As	1.26(−10)	1.47(−10)	1.25(−10)	1.28(−10)	6.22(−11)	1.10(−10)	5.21(−12)	6.30(−12)	1.39(− 6)	1.60(− 5)	4.78(− 5)	1.02(− 4)	1.90(− 4)	3.13(− 4)
^{74}Se	4.10(−12)	3.25(− 9)	4.09(− 9)	4.65(− 9)	2.55(− 9)	4.98(− 9)	2.54(−10)	6.09(− 9)	2.01(− 3)	2.24(− 2)	6.64(− 2)	1.41(− 1)	2.62(− 1)	4.30(− 1)
^{76}Se	3.39(−10)	6.41(−10)	5.39(−10)	5.30(−10)	2.29(−10)	3.96(−10)	1.61(−11)	1.06(−11)	1.75(− 6)	2.32(− 5)	7.50(− 5)	1.69(− 4)	3.38(− 4)	6.06(− 4)
^{77}Se	1.71(−10)	8.40(−11)	7.63(−11)	8.00(−11)	3.91(−11)	7.12(−11)	3.26(−12)	1.67(−12)	6.80(− 9)	9.68(− 8)	3.23(− 7)	7.39(− 7)	1.47(− 6)	2.56(− 6)
^{82}Se	2.43(− 9)	1.19(− 9)	1.01(− 9)	1.02(− 9)	4.39(−10)	8.51(−10)	2.72(−11)	1.20(−11)	6.29(−10)	5.66(−10)	1.32(−12)	9.94(−11)	2.79(−11)	3.73(−12)
^{79}Br	1.75(−10)	1.43(−10)	1.35(−10)	1.39(−10)	6.52(−11)	1.19(−10)	4.94(−12)	2.41(−12)	3.51(− 9)	5.24(− 8)	1.80(− 7)	4.17(− 7)	8.50(− 7)	1.53(− 6)
^{81}Br	6.16(−10)	6.16(−10)	5.58(−10)	5.72(−10)	2.55(−10)	4.83(−10)	1.71(−11)	7.83(−12)	3.66(−10)	5.31(−10)	7.96(−10)	1.98(− 9)	4.01(− 9)	7.28(− 9)
^{78}Kr ...	8.50(−25)	8.00(−10)	1.92(− 9)	2.75(− 9)	1.87(− 9)	4.66(− 9)	2.18(−10)	1.25(−10)	6.39(− 9)	1.54(− 8)	3.25(− 8)	7.61(− 8)	1.53(− 7)	2.77(− 7)
^{80}Kr ...	4.42(−19)	1.58(− 9)	2.89(− 9)	3.51(− 9)	1.91(− 9)	4.24(− 9)	1.63(−10)	8.18(−11)	4.85(− 8)	7.71(− 7)	2.76(− 6)	6.58(− 6)	1.37(− 5)	2.52(− 5)
^{83}Kr ...	6.48(−10)	4.23(−10)	3.82(−10)	3.94(−10)	1.64(−10)	3.47(−10)	9.38(−12)	4.08(−12)	2.91(−10)	6.14(−10)	1.36(− 9)	3.38(− 9)	7.05(− 9)	1.31(− 8)
^{84}Sr	6.77(−22)	1.54(−10)	6.12(−10)	1.03(− 9)	8.28(−10)	2.80(− 9)	1.11(−10)	6.58(−11)	5.67(− 9)	1.94(− 8)	5.47(− 8)	1.40(− 7)	3.03(− 7)	5.83(− 7)

NOTE.—Table 4 is also available in machine-readable form in the electronic edition of the *Astrophysical Journal*.

low a density for much additional electron capture or positron decay (Arnett & Truran 1969; Truran & Arnett 1971; Arnett 1973).

This neutron deficiency imprints a distinctive signature on the nucleosynthesis of Population III pair-instability supernovae that is even more extreme than seen in metal-free stars of lower mass.

3.3. *Integrated Nucleosynthesis*

In Figure 3, the individual isotopes in Table 1 have been summed, divided by the mass ejected (equal to the mass of the star in the present study), and the resultant elemental mass fraction integrated over an estimated Salpeter-like (Salpeter 1959) IMF for the assumed progenitor stars of the helium cores (§ 3.1) and divided by their solar mass fraction. We show the result of this integration for three different slopes, $\gamma = -0.5$, -1.5, and -3.5 of the IMF, where γ is defined by the number of stars formed per mass interval, $\gamma \equiv 1 + d \log N/d \log M$. The "dot" indicates the middle value, connected by lines, and the "thick" and "thin" ends of the triangle show the shallower and steeper IMF slopes, respectively.

The results, shown in Figure 3, are not very sensitive to the slope of the IMF since we are only studying stars in a limited mass range (a factor of 2 from the lowest to the highest mass considered). The dependence of the integrated production factor on the element number Z shows the odd-even effect discussed in § 3.2 and quantifies it to be from 1 order of magnitude for iron group elements to 2 orders of magnitude for some of the intermediate-mass elements. The iron group shows a smaller effect because of the weak interactions that occur in the central regions of the more massive cores because they reach high density during their bounce.

Given the unusual nature of the synthesis site (pair instability supernovae are not generally thought to be the dominant site where solar abundances were produced), the overall approximate agreement of the yields with the solar abundances of elements with even charge is somewhat surprising. The nuclear properties of the elements—their binding energies and cross sections—are apparently as important as the stellar environment. However, there are differences. For example, Si and S are overabundant compared to O, Fe, and Mg. As noted in § 3.2, elements above Ni are essentially absent. Above Ge, the numbers are all below the lower bound of the plot, and their abundance decreases exponentially with mass number.

This conflicts with observations that show appreciable r-process elements present even in very metal-deficient stars (see, e.g., Burris et al. 2000), at least for [Fe/H] $\gtrsim -2.9$. Since we believe that the r-process requires neutron stars—one way or another—for its production, the synthesis of elements by lower mass stars must also be considered. That is, no matter what the IMF for Population III, abundances at [Fe/H] $\gtrsim -3$ could not have been made solely by pair-instability supernovae.

Also, lacking any hard evidence of what the IMF for Population III was like, one cannot preclude a truncation somewhere within the mass range $M_{\rm He} = 64, \ldots, 133\ M_\odot$. Taking away the stars above $M_{\rm He} = 90\ M_\odot$ could clearly give an arbitrarily large production factor for oxygen and intermediate-mass elements compared to the iron group.

To explore further the consequences of an admixture of lighter Population III stars, we included in our integration the yields of the "Z series" of Population III supernovae studied by Woosely & Weaver (1995), metal-free stars in the mass range 12–40 $M_\odot$. Figures 4 and 5 show the consequences of including these stars with two different choices of explosion energy. For larger explosion energies, less fallback occurs, and more iron group elements are ejected. In the higher mass stars that tend to make black holes, more explosion energy ejects more heavy elements of all kinds. This explains the difference between Figures 4 and 5. We also assume, as the calculations suggest, that for reasonable supernova energies, no heavy elements are ejected in the explosion of Population III stars over 40 $M_\odot$ (Fryer 1999).

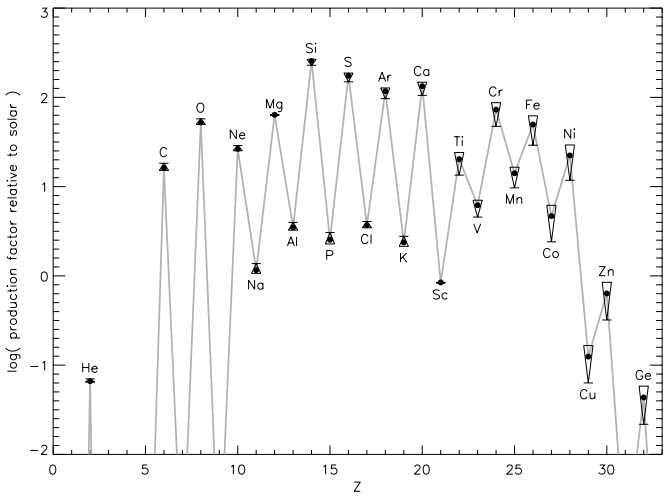

FIG. 3.—Production factors for very massive stars (helium cores of 65–130 $M_\odot$, corresponding to initial masses of ~140–260 $M_\odot$) integrated over an IMF and compared to solar abundances as a function of element number Z. The integration assumed a Salpeter-like IMF with three different exponents: -0.5 (*thick end of triangle*), -1.5 (*solid dot*), and -3.5 (*thin end of triangle*).

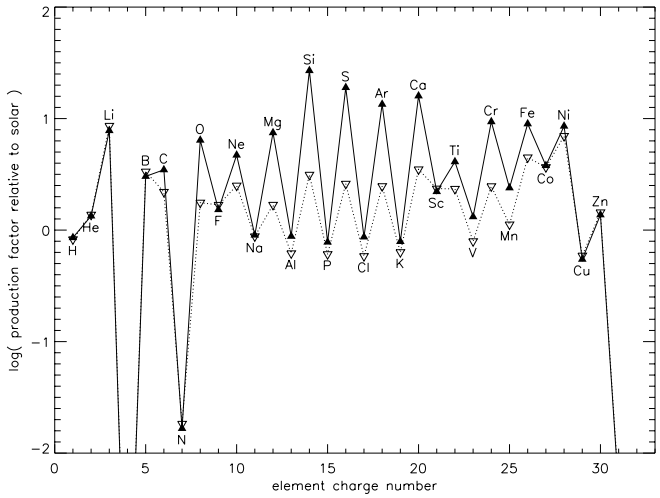

FIG. 4.—Production factors for massive stars (12–40 $M_\odot$; *dotted line, open triangles*) integrated over IMF and compared with solar abundances as a function of element number. The yields are taken from Woosely & Weaver (1995), and in this plot we use the low explosion energy primordial models of the "A" series, Z12A, Z15A,.... The solid line and filled triangles give the same integration but also including exploding very massive stars (~140–260 $M_\odot$). In the mass range 40–100 $M_\odot$ essentially the whole helium core falls into a black hole, ejecting only the unprocessed envelope. In the mass range 100–140 $M_\odot$ some of the outer layers of the helium core may be ejected, adding to the carbon and oxygen yields and maybe a little to the neon and magnesium yields but not to the heavier elements. The IMF is assumed Salpeter-like with an exponent of -1.5.

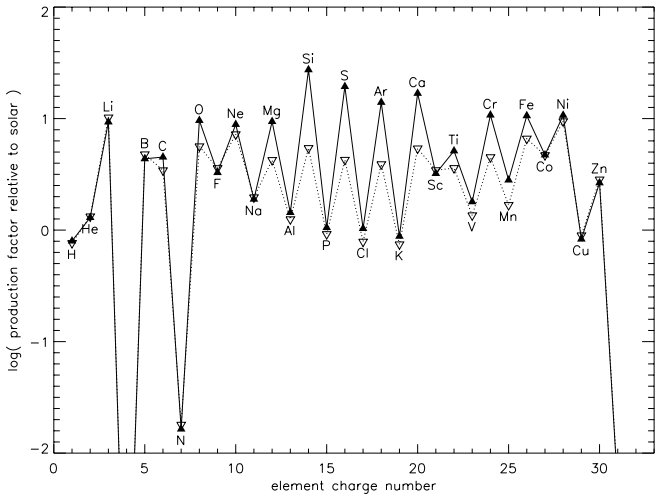

FIG. 5.—Same as Fig. 4, but here we used the high-energetic explosion of the "B" series from Woosely & Weaver (1995) for 25 $M_\odot$ and above, Z25B, Z30B,....

This is in part because very little mass loss occurs, and the star dies while still having a large helium core.

The figures show, not too surprisingly, that including the "lower mass" supernovae tends to wash out the dramatic odd-even effect seen in the pair instability supernovae. Still the two mass ranges, $M_{\rm ZAMS} = 12$–40 and 140–260, make approximately the same total masses of heavy elements. The lighter stars are more abundant in a Salpeter IMF, but they eject less mass—both because they are themselves less massive and because of fallback. The modification introduced by a pair-unstable massive component may have observational consequences so long as the high-mass component continues to form. Of course, the formation of pair-unstable objects may cease after the creation of only a small metallicity (Baraffe et al. 2001).

3.4. *Some Specific Nuclei*

3.4.1. *Li, B, F*

These fragile light nuclei are made only (in our calculations) by the neutrino process in stars lighter than about 40 $M_\odot$. They are not produced in pair instability supernovae

3.4.2. *Nitrogen*

An important issue in very metal-deficient stars is the production of primary nitrogen (see, e.g., Norris, Ryan, & Beers 2001). In this paper we have studied only helium cores and thus will have missed any nitrogen production that occurs when the helium convective shell and hydrogen envelope of these same massive stars mix (Woolsey & Weaver 1982). We hope to return to this matter in a future publication but note for now the sensitivity of the results to uncertain parameters of convective overshoot and rotationally induced mixing (Woosely & Weaver 1995; Heger et al. 2000a, 2000b; Umeda, Nomoto, & Nakamura 2000). It may also be possible to produce primary nitrogen in asymptotic giant branch (AGB) stars (Ventura et al. 2001; P. A. Denissenkov & A. Weiss 2002, in preparation).

3.4.3. *Zinc*

Very little zinc is produced in the pair instability explosions. What is made is produced chiefly as ^{64,66}Zn made as ^{64,66}Ge in an extreme α-rich freeze out at the upper end of the mass range that explodes. However, one does expect zinc production in the neutrino-powered wind just after the shock is launched in the deepest layers of stars between about 10 and 20 $M_\odot$ (Hoffman et al. 1996), essentially the same site as the *r*-process. This neutrino wind was not included either in the present calculation or that of Woosely & Weaver (1995) but could easily give a much higher prediction for zinc.

3.4.4. *The r- and s-Processes*

Because of the lack of any heavy seed nuclei or any appreciable neutron source in helium burning, there is no *s*-process in low-metallicity pair-instability supernovae. Also, because no neutron star is formed and no shock wave passes through any region where appreciable electron capture has occurred, there is no *r*-process. This latter conclusion might possibly be altered in rapidly rotating pair-unstable stars that produce black holes, accretion disks, and jets.

However, the simplest explanation of *r*-process abundances in metal-deficient stars is that they indicate the contribution of an additional nucleosynthetic component—namely, those lower mass stars that make regular supernovae and neutron stars.

4. CONCLUSIONS AND OBSERVATIONAL TESTS

The natural places to look for the distinctive nucleosynthetic pattern of pair instability supernovae is in the stellar photospheres of very metal-deficient stars nearby and in damped Lyα systems at high redshift. However, to truly see the signature of Population III, one must go to very low metallicities. It is estimated by Baraffe et al. (2001) that the stars responsible for pair instability supernovae are already significantly pulsationally unstable when the metallicity has risen to as little as $Z \sim 10^{-4}$ solar (the lowest nonzero metallicity investigated by Baraffe et al. 2001; the stellar structure changes significantly between $Z/Z_\odot = 0$ and 10^{-4}).

Studies of giant stars in the Milky Way are beginning to push the frontier to [Fe/H] $= -4$ (McWilliam et al. 1995; Ryan, Norris, & Beers 1996; Norris et al. 2001; Giridhar et al. 2001) and reveal some interesting tendencies—some expected and some surprising. One of the most striking is the dramatic decrease of [Al/Fe] (or [Al/Mg]) at very low metallicity. Without non-LTE corrections, the deficiency approaches 1.5 dex (Norris et al. 2001) and would strongly suggest a pair instability contribution (Fig. 4). However, estimated corrections bring the Al abundance up and into better accord with what is expected from ordinary supernovae. The α-elements, Mg, Si, and Ca, are clearly up by 0.3–0.5 dex at low metallicity, consistent with pair instability supernovae but not inconsistent with regular supernovae either. The fact that [Ti/Fe] is up by the same amount is surprising in any case. Perhaps it is not so much that these intermediate-mass elements are up as it is Fe that is down—because of a lack of Type Ia supernovae. Even more intriguing is the *overproduction* of [Co/Fe] at low metallicities, which is difficult to understand in any model. Production of Co occurs by the α-rich freeze out and can be enhanced by high temperatures and rapid expansion. Perhaps we are seeing evidence of deeper bounces in pair-unstable stars in which rotation was important, but then one would expect other elements made from the α-rich

freeze out, like Ni, also to be enhanced, and they are not. A plot of [Mn/Fe] versus [Fe/H] shows a clear decrease from nearly solar at [Fe/H] = −2 to about [Mn/Fe] = −1 at [Fe/H] = −3.5 (Giridhar et al. 2001). This is consistent with pair instability supernovae but, again, not inconsistent with what core collapse supernovae alone could do (Figs. 4 and 5; see also Nakamura et al. 1999).

More measurements, and more precise measurements of abundances at [Fe/H] ≈ -4, would help as well as a better understanding of the non-LTE corrections involved in the spectral analysis. Particularly sensitive to our stellar models are the ratios of pairs of elements separated by one proton: [Na/Mg], [Al/Mg], [Al/Si], [P/S], [P/Si], [Cl/S], [K/Ca], and the like. One should keep in mind, though, that a single pair instability explosion that produced 40 $M_\odot$ of iron could provide all the iron necessary for [Fe/H] = −4 in 4×10^8 $M_\odot$ of primordial material. A + [Fe/H] = 4 mixing probably is not so efficient at [Fe/H] = −4 that we do not sample individual events. It is thus possible to get *very* large excursions in ratios like [Si/Fe], [O/Fe], etc., even in stars where [O/Fe] is greatly *subsolar*—see the individual entries in Table 3. The effects shown in Figures 3, 4, and 5 may need to be applied to a statistically large sample of stars at [Fe/H] = −4. We understand that this may be challenging.

Abundances in damped Lyα systems are also starting to be measured for heavy elements. Lu et al. (1996) and Prochaska & Wolfe (1999, 2002) have measured abundances in damped Lyα systems for redshifts <1.5 and metallicity down to about [Fe/H] = −2. The abundance trends in these systems have similarities to, but are not the same as in, metal-deficient halo stars (Prochaska & Wolfe 2002). As in halo stars, there is a tendency for Si/Fe to be significantly enhanced at low metallicity, up to 0.6 dex. Similar enhancements are seen in S and Ar. Si/Al also rises with decreasing metallicity, but the effect is not so large as seen in halo stars, less than 0.5 dex rather than 1.0 dex. Also, unlike in halo stars, there is no clear depletion of Cr at low metallicity. In fact, it may be slightly enhanced. All these effects, except the weak deficiency of Al, are consistent with a pair-instability supernova contribution (e.g., with the solid line in Fig. 4), but interpretation is complicated by the small range of metallicity sampled, possible depletion into dust, and a time-varying contribution of Type Ia supernovae. What is needed are more measurements of odd-Z elements (Al, P, and Mn might be candidates) at still smaller metallicities, although this too will be challenging.

We are grateful to Chris Fryer for discussions about Figure 2. This research has been supported by the NSF (AST 97-316569), the DOE ASCI Program (B347885), and the Alexander von Humboldt-Stiftung (FLF-1065004).

REFERENCES

Abel, T. G., Bryan, G. L., & Norman, M. L. 2000, ApJ, 540, 39
Arnett, W. D. 1973, ARA&A, 11, 73
Arnett, W. D., & Truran, J. W. 1969, ApJ, 157, 339
Baraffe, I., Heger, A., & Woosley, S. E. 2001, ApJ, 550, 890
Barkat, Z., Rakavy, G., & Sack, N. 1967, Phys. Rev. Lett., 18, 379
Bond, J. R., Arnett, W. D., & Carr, B. J. 1984, ApJ, 280, 825
Bromm, V., Coppi, P. S., & Larson, R. B. 1999, ApJ, 527, L5
Buchmann, L. 1996, ApJ, 468, L127 (and erratum 479, L153 [1997])
Burris, D. L., Pilachowski, C. A., Armandroff, T. E., Sneden, C., Cowan, J. J., & Roe, H. 2000, ApJ, 544, 302
Caughlan, G. A., & Fowler, W. A. 1988, At. Data Nucl. Data Tables, 40, 283
Davidson, K., et al. 1999, AJ, 118, 1777
Ezer, D., & Cameron, A. G. W. 1971, Ap&SS, 14, 399
Filippenko, A. V., Barth, A. J., Bower, G. C., Ho, L. C., Stringfellow, G. S., Goodrich, R. W., & Porter, A. C. 1995, AJ, 110, 2261
Fryer, C. L. 1999, ApJ, 522, 413
Fryer, C. L., Woosley, S. E., & Heger, A. 2001, ApJ, 550, 372
Giridhar, S., Lambert, D. L., Gonzales, G., & Pandey, G. 2001, PASP, 113, 519
Glatzel, W., Fricke, K. J., & El Eid, M. F. 1985, A&A, 149, 413
Heger, A., Baraffe, I., Fryer, C. L., & Woosley, S. E. 2001, Nucl. Phys. A, 688, 197
Heger, A., Langer, N., & Woosley, S. E. 2000a, ApJ, 528, 368
Heger, A., Woosley, S. E., Waters, R. 2000b, The First Stars, ed. A. Weiss, T. G. Abel, & V. Hill (Berlin: Springer), 121
Hoffman, R. D., Woosley, S. E., Fuller, G. M., & Meyer, B. S. 1996, ApJ, 460, 478
Iglesias, C. A., & Rogers, F. J. 1996, ApJ, 464, 943
Kudritzki, R.-P. 2000, in The First Stars, ed. A. Weiss, T. G. Abel, & V. Hill (Berlin: Springer), 127
Kunz, R., Jaeger, M., Mayer, A., Hammer, J. W., Staudt, G., Harissopulos, S., & Paradellis, T. 2001, Phys. Rev. Lett, 87, 202,501
Larson, R. B. 2000, in Star Formation from the Small to Large Scale, ed. F. Favata, A. A. Kaas, & A. Wilson (ESP SP-445; Noordwijk: ESA), 13
Lu, L., Sargent, W. L. W., Barlow, T. A., Churchill, C. W., & Vogt, S. S. 1996, ApJS, 107, 475
McWilliam, A., Preston, G. W., Sneden, C., & Searle, L. 1995, AJ, 109, 2757
Nakamura, F., & Umemura, M. 2001, ApJ, 548, 19
Nakamura, T., Umeda, H., Nomoto, K., Thielemann, F.-K., & Burrows, A. 1999, ApJ, 517, 193
Norris, J. E., Ryan, S. G., & Beers, T. C. 2001, ApJ, 561, 1034
Ober, W. W., El Eid, M. F., & Fricke, K. J. 1983, A&A, 119, 61
Ostriker, J. P., & Gnedin, N. Y. 1996, ApJ, 472, L63
Prochaska, J., & Wolfe, A. 1999, ApJS, 121, 369
———. 2002, ApJ, 566, 68
Rakavy, G., Shaviv, G., & Zinamon, Z. 1967, ApJ, 150, 131
Rauscher, T., Heger, A., Hoffman, R. D., & Woosley, S. E. 2002, ApJ, submitted (astro-ph/0112478)
Ryan, S. G., Norris, J. E., & Beers, T. C. 1996, ApJ, 471, 254
Salpeter, E. E. 1959, ApJ, 129, 608
Stringfellow, G. S., & Woosley, S. E. 1988, in The Origin and Distribution of the Elements, ed. G. J. Mathews (Singapore: World Scientific), 467
Thielemann, F.-K., Nomoto, K., & Hashimoto, M. 1996, ApJ, 460, 408
Truran, J. W., & Arnett, W. D. 1971, Ap&SS, 11, 430
Umeda, H., Nomoto, K., & Nakamura, T. 2000, in The First Stars, ed. A. Weiss, T. G. Abel, & V. Hill (Berlin: Springer), 150
Ventura, P., D'Antona, F., Mazzitelli, I., & Gratton, R. 2001, ApJ, 550, L65
Vink, J. S., de Koter, A., & Lamers, H. J. G. L. M. 2001, A&A, 369, 574
Weaver, T. A., Zimmerman, G. B., & Woosley, S. E. 1978, ApJ, 225, 1021
Wilson, J. R., Mayle, R., Woosley, S. E., & Weaver, T. A. 1986, in Ann. NY Acad. Sci., 470, Proceedings of the 12th Texas Symposium, ed. M. Livio & G. Shaviu, 267
Woosley, S. E. 1986, in Nucleosynthesis and Chemical Evolution, ed. B. Hauck, A. Maeder, & G. Meynet (Switzerland: Geneva Obs.), 1
Woosley, S. E., & Weaver, T. A. 1982, in Supernovae: A Survey of Current Research, ed. M. J. Rees & R. J. Stoneham (Dordrecht: Reidel), 79
———. 1995, ApJS, 101, 181